ELSEVIER

Polymer 43 (2002) 5271–5279

polymer

www.elsevier.com/locate/polymer

Simultaneous presence of positive and negative spherulites in syndiotactic polystyrene and its blends with atactic polystyrene

Chi Wang*, Chao-Chen Chen, Yong-Wen Cheng, Wei-Po Liao, Min-Ling Wang

Department of Chemical Engineering, National Cheng Kung University, Tainan 701, Taiwan, ROC

Received 4 February 2002; received in revised form 17 May 2002; accepted 31 May 2002

Abstract

Crystal growth rates of syndiotactic polystyrene (sPS) and its blends with atactic polystyrene (aPS) at various temperatures (T_c) were measured using a polarized optical microscope (POM). In addition to the positively birefringent spherulites and axilites (P-spherulites and P-axilites) which are predominantly observed, small population of negatively birefringent spherulites (N-spherulites) is also detected in the neat sPS as well as in the sPS/aPS blends at a given T_c. Both P-spherulites and P-axilites possess a similar growth rate, whereas a smaller growth rate is found for N-spherulites at all T_c and samples investigated. Melting behavior of individual P- and N-spherulites was feasibly traced using hot-stage heating and a highly sensitive CCD through the decay of transmitted light intensity under cross-polars. Both P- and N-spherulites demonstrate exactly the same melting behavior under POM, which well corresponds to the differential scanning calorimetry measurements, suggesting no difference in lamellar thickness distribution or crystal perfection within P- and N-spherulites. Lamellar morphologies within spherulites were extensively investigated using transmission electron microscopy (TEM) as well as scanning electron microscopy (SEM). Results obtained from TEM and SEM show that the lamellar stacks within P-spherulites grow radially, whereas those within N-spherulites are packed relatively tangentially. The growth of P-spherulites is associated with the gradual increase of lamellae' lateral dimensions which follows the conventional theory of growth mechanism. However, the measured growth rate of N-spherulites is relevant to the gradual deposition of new lamellar nuclei adjacent to the fold surfaces of already-existing lamellar stacks. The difference in measured growth rate between P- and N-spherulites is attributed to the different energy barrier required to develop stable nuclei. Based on the exhaustive TEM and SEM observations, plausible origin of N-spherulites is provided and discussed as well.

Keywords: Syndiotactic polystyrene; Negative spherulite; Melting

1. Introduction

Recently, many studies [1–10] have been conducted on the crystal characterization and crystallization of syndiotactic polystyrene (sPS) due to its unique properties including high melting temperature and good chemical resistance. Owing to the stereoregularity of the backbone chains, sPS is able to crystallize and several polymorphs have been reported. Moreover, it possesses a faster crystallization rate, compared to its isotactic counterpart (iPS) at a fixed undercooling [11]. At the micrometer scale, spherulitic morphology is usually observed for sPS and its blends with other polymers. Although growth rate of sPS spherulites have been measured several times on neat sPS and its blends with atactic polystyrene (aPS) [12], polyvinyl methyl ether (PVME) [13] and poly(2,6-dimethyl-p-phenylene oxide) (PPO) [12,14], the birefringent characters of sPS spherulites resulting from difference in refractive index along the radial and tangential directions are seldom reported. It is well known that anisotropic characters exist within spherulites, leading to the difference in the refractive index along the radial (n_r) and tangential (n_t) directions. When n_r is larger than n_t, i.e. $\Delta n = n_r - n_t > 0$, a positively birefringent spherulite (P-spherulite) is developed. On the other hand, a negatively birefringent spherulite (N-spherulite) gives a larger refractive index in the tangential direction, compared to that in the radial direction. Values of n_r and n_t are mainly dependent on the relative orientation of crystals within spherulites since refractive index along the three lattice axis are generally different from one another. To the best of the authors' knowledge, there was only one article up to date to describe the birefringent characters of the sPS spherulites in Ref. [13]. Simultaneous presence of P- and N-spherulites has been reported only once by Cimmino

* Corresponding author. Fax: +886-6-2344496.
E-mail address: chiwang@mail.ncku.edu.tw (C. Wang).

0032-3861/01/$ - see front matter
PII: S0032-3861(02)00351-8

et al. [13] on studying the spherulitic growth of sPS/PVME blends. They found that the growth rate of P-spherulites is larger than that for N-spherulite at a given crystallization temperature. In the neat sPS system, however, they discovered both P-spherulites and P-axilites (sheaf-like structure) only and no N-spherulites were detected. They concluded that occurrence of sPS N-spherulites is due to heterogeneous nucleation by the presence of the foreign PVME polymer. No detailed microstructure inside individual spherulites was provided to account for the difference in the birefringent characters. Recently, simultaneous presence of P- and N-spherulites is also observed by us in the sPS/aPS blends as well as in the neat sPS system. In the present article, growth rate and melting behavior of these individual spherulites are examined. In addition, lamellar morphologies within spherulites are probed using transmission electron microscopy (TEM) and scanning electron microscopy (SEM) to elucidate the origin which leads to the birefringence difference among sPS spherulites.

2. Experimental

sPS pellets with a weight average molecular weight (M_w) of 200 kg/mol was supplied by Dow Chemical, USA. aPS with a M_w of 100 kg/mol was purchased from Aldrich Co. To prepare sPS/aPS blend (50/50 by weight ratio), appropriate amounts of aPS and sPS were first dissolved in *ortho*-dichlorobenzene (*o*-DCB) at 140 °C for 2 h with a polymer concentration of 1 wt%. The homogeneous solution was then poured into 20 fold excess volume of methanol for precipitation of sPS/aPS blend powders. The powders of sPS/aPS blend were collected through filtration and vacuum dried at 150 °C for 40 h to remove the residual solvents. Thin films of neat sPS (and sPS/aPS blends) were made using press molding at 290 °C and 0.6 MPa for 10 min and then cooled slowly (ca. −7.0 °C/min) at atmosphere pressure. According to our previous findings, the as-molded samples were crystallized into β′ crystal lattice characterized by wide-angle X-ray diffraction (WAXD) and FTIR spectrums [15].

A polarized optical microscope (POM, Leica DMLP) equipped with a hot stage (THMS600, Linkam) was used to observe the growth of spherulites during isothermal crystallization. Prior to measurements, the hot stage was calibrated with benzoic acid. The samples were first to maintain at 300 °C for 10 min and then quickly cooled to the desired temperature (T_c) for crystallization. Radii of growing spherulites were measured continuously through a recording system until the impingement of spherulites. The slope of spherulitic radius versus elapsed time gave the crystal growth rate. In addition to the spherulites, axilites were observed as well especially at high T_c. For axilitic crystals, the growth of the major axis was monitored as a function of time. Then, the crystal growth rate was determined from the slope of a plot of half-major axis versus elapsed time. A λ compensator was frequently used to characterize the birefringence of the spherulites developed. After crystallization, visual observations of melting behavior of spherulites at a heating rate of 10 °C/min were carried out on the POM equipped with an AP1 camera (Apogee Instruments Inc.) to measure the light intensity as well. The camera possesses 16-bit dynamic range charge coupled detector (CCD) with a resolution of 768 × 512 pixels. Automatic storage of the images was conducted by a recording system at a time interval of 2.8 s, leading the temperature resolution to be 0.24 °C of accuracy. Under cross-polars, the high-performance CCD imaging system will give the intensity change of transmitted light of selected regions enclosing the desired spherulite separately. The transmitted light intensity was thus monitored as a function of time first and transformed to the corresponding temperature later, depending on the heating rate. In this manner, the melting behavior of individual spherulites can be probed as a function of temperature. In addition, melting behavior of sPS samples was investigated as well using a differential scanning calorimeter (DSC, Perkin Elmer DSC7). The sample loaded was ca. 8 mg and heating was conducted from T_c to 300 °C at a rate of 10 °C/min. The thermal condition for samples to crystallize isothermally in DSC pans was the same as that used for POM observations.

TEM was conducted to reveal the lamellar morphology of the crystallized samples. Ultrathin films (ca. 50 nm) were prepared using a microtome (ULTRACUT, Leica) at room temperature and were collected on 200 mesh copper grids. Then, the films were exposed to the vapor of RuO_4 to enhance the contrast between amorphous and crystalline layers [16] under TEM (Jeol, JEM-1200EX) observation operated at an accelerating voltage of 80 kV. Fresh staining solution was prepared by dissolving 20 mg of ruthenium dioxide and 10 mg of sodium periodate in 3 ml of saturated sodium periodate aqueous solution. The clear golden yellow solution containing RuO_4 was used immediately for a better staining efficiency. Morphology of lamellar stacks of sPS/aPS blends was also investigated using SEM, Hitachi S4100. Prior to SEM observation, the isothermally-crystallized thin films were etched using amyl acetate to wash away the aPS component. The etching procedure followed the method proposed by Kit and Schultz [17]. SEM images of the residual sPS lamellar stacks were recorded at 100 kV.

3. Results and discussion

Under POM observations, three different morphologies at the micrometer scale are evidently observed for neat sPS and sPS/aPS blends after melt crystallization, i.e. positively birefringent spherulites (P-spherulites), positively birefringent axilites (P-axilites) and negatively birefringent spherulites (N-spherulites). This is similar to sPS/PVME blends but different from the neat sPS system observed by Cimmino et al. [13] where only P-spherulites and P-axilites

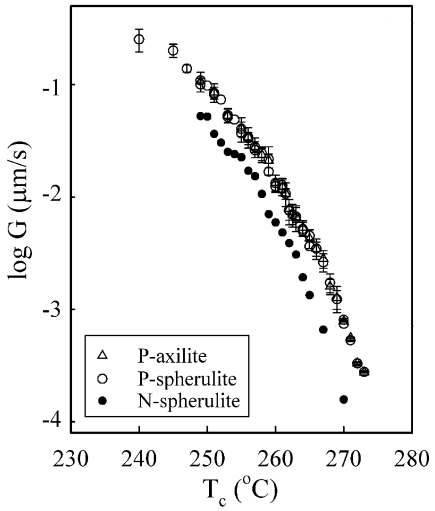

Fig. 1. Crystal growth rate of neat sPS at various crystallization temperatures.

were found. From the plots of growing crystal size versus elapsed time for these three morphologies, a linear growth rate was always detected for neat sPS as well as sPS/aPS blends. Heterogeneous nucleation is expected since almost simultaneous appearance of crystal nuclei is observed at the early stage of crystallization. A careful visual examination, however, leads to the fact that P-spherulites and P-axilites appear relatively earlier than N-spherulites. Moreover, N-spherulites show dimmer character of depolarized light than P-spherulites (or P-axilites) under cross-polars, suggesting a less birefringent level within N-spherulites. Fig. 1 shows the variation of the measured growth rates with the crystallization temperature for these three morphologies in the neat sPS system. As the T_c is increased, the crystal growth rate decreases as expected due to the difficulty in forming stable nuclei at high T_c. Both P-axilites and P-spherulites possess the same growth rate at all the T_c investigated. It is of interest to note that a smaller growth rate is obtained for N-spherulites at a given T_c, compared to P-spherulites. Similar results were obtained for 50/50 blends and were not shown here for brevity. However, the crystal growth rate in sPS/aPS blends is reduced at all given T_c, when compared to that of neat sPS. Detailed discussion of the aPS effect on the crystallization kinetics and growth rate of sPS will be provided in our future article.

Crystal modification of the studied samples was characterized using WAXD and the diffraction peaks were found well corresponding to those for β′-form crystals exclusively. Thus, the possibility for different crystal lattice which is often observed in sPS due to its polymorphic nature is excluded from accounting for the presence of spherulites with different birefringence. Fig. 2 gives the fraction of the crystal density for these three morphologies at various T_c. Crystal number of each type was counted at a magnification of 100 × and ca. 1000 crystals in total were accumulated to give comparative plots in Fig. 2. Majority of sPS crystals are in the form of either P-spherulites or P-axilites and only

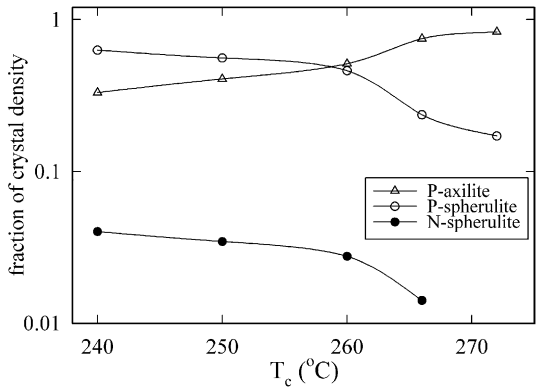

Fig. 2. Fraction of crystal density as a function of crystallization temperature for neat sPS.

small percentage of N-spherulites, ca. 4%, is found. As T_c is increased, more P-axilites are developed and fraction of spherulitic features is gradually reduced. It seems that spherulitic features are predominant at low T_c, whereas axilitic morphology is preferred at high T_c. Indeed, the P-axilites observed under POM are under-developed sheaf-like structure probed by TEM (as discussed later). Fig. 3 gives the final spherulitic radius of P- and N-spherulites at various T_c. As T_c is increased, the number of nuclei is slightly decreased, leading to a relatively larger spherulitic radius at high T_c. Moreover, the radius of N-spherulites is only about half of that for P-spherulites due to the late appearance and slow growth. To probe lamellar orientation within spherulites so as to characterize the spherulitic birefringence, micro-beam X-ray diffraction is frequently conducted [18,19]. However, the diameter of sPS is relatively small, ca. 30 and 15 μm at most for P- and N-spherulites, respectively, as shown in Fig. 3. It is very difficult if in principle not impossible to probe the internal structure of sPS spherulites using micro-beam X-ray of which the beam size has to be sufficiently small to enclose individual spherulites.

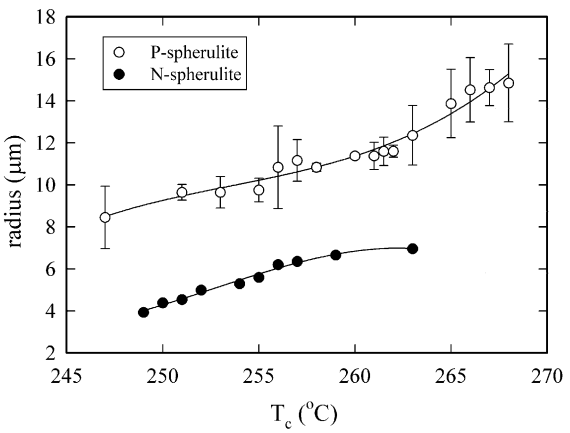

Fig. 3. Final radius of spherulites as a function of crystallization temperature for neat sPS.

3.1. Melting behavior of individual spherulites

Conventionally, melting behavior of crystallized polymers has been widely conducted on DSC to determine the melting temperature and further reveal the thickness and perfection of lamellae which are the sub-structure of the spherulites (or axilites). It has been established from DSC measurements on neat sPS and sPS/aPS blends that two melting peaks are found at low T_c, whereas one melting peak is detected at high T_c [15,20]. Since the present samples are all crystallized into orthorhombic β′ modification exclusively, the possibility of different crystal lattices (polymorph), i.e. the coexistence of α and β crystals, to render the double-melting behavior is ruled out. Double-melting behavior has also been observed for nylon 6,6, resulting from the melting of the two types of spherulites but not the polymorph [21,22]. It has been found that P-spherulites of nylon 6,6 are developed at T_c lower than 251 °C. Nevertheless, N-spherulites and spherulitic aggregates of nylon 6,6 grow at T_c higher than 251 °C. Gradual melting of P-spherulites and transformation to N-spherulites takes place during heating nylon 6,6 samples crystallized at a temperature lower than 251 °C, leading to the double-melting behavior. For nylon 6,6, the lower melting temperature is associated with the melting of P-spherulites, whereas the higher melting temperature is relevant to the melting of N-spherulites. The transformation of birefringence characters, however, either from P- to N-spherulites or from N- to P-spherulites is not detected for sPS as well as sPS/aPS blends from our extensive POM observations.

Now, for sPS and its blends with aPS systems, a crucial question is: what accounts for the presence of the double-melting behavior of sPS? Is it due to the simultaneous presence of P- and N-spherulites? In other words, can it be attributed to the melting of the spherulites of first kind, followed by the melting of second type? To clarify the melting behavior of individual spherulites (or axilites), it is desirable to observe sPS crystal melting under POM at the same heating rate applied on DSC measurements. However, the heating rate applied has to be sufficiently high to reduce the effect of recrystallization and/or reorganization during heating. To faithfully follow the melting behavior of sPS at a high heat rate (10 °C/min), a high-performance CCD camera used for precise measurements of light intensity is preferred during heating. Under the cross polar condition, the crystals within samples will rotate the light passing already through the polarizer to certain level, leading portion of transmitted light to be parallel to the analyzer which can be measured by the CCD camera. On the other hand, no transmitted light can pass the analyzer and be detected by the CCD camera if there is no crystal existing in the samples. Thus, its is considered that the level of crystallinity within spherulites is proportional to the intensity of transmitted light measured [23,24].

On heating of a selected spherulite, the transmitted light intensity should decrease gradually due to the melting of sPS crystals within the spherulite until a threshold intensity for background is reached where the spherulite is completely melted. Figs. 4 and 5 are the results measured in this manner for sPS and sPS/aPS blends which are melt-crystallized at 241 and 252 °C, respectively, prior to the heating scans. Vertical shift of plots was conducted for a clear comparison of melting behavior for different spherulites. For neat sPS crystallized at 241 °C, pronounced melting starts at 257.6 °C where a significant reduction of transmitted light is detected. Melting continues until at a temperature 259.9 °C where an upturn of the light intensity is seen, rising to reach a maximum intensity at 263.7 °C. After 263.7 °C, a gradual diminution in light intensity is evident again until the complete melting of sPS spherulites at 273.1 °C. Both P- and N-spherulites show the same profiles of measured light intensity, indicating a similar melting behavior. The upturn of measured intensity in Fig. 4(a) suggests the increase of crystallinity within spherulites and implies the reorganization and/or recrystallization of imperfect sPS crystals into more perfect ones. Fig. 4(b) shows the measured intensity profiles for 50/50 blends during heating. A pronounced two-step drop in

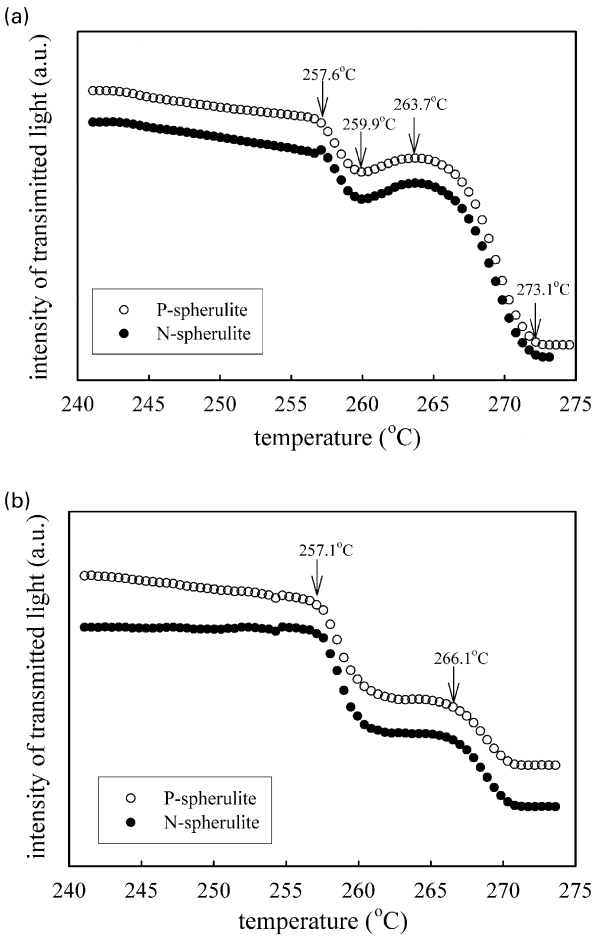

Fig. 4. Variation of the transmitted light intensity of P-spherulites and N-spherulites during heating of (a) neat sPS and (b) sPS/aPS = 50/50 blends melt-crystallized at T_c = 241 °C. (cross-polars, heating rate = 10 °C/min).

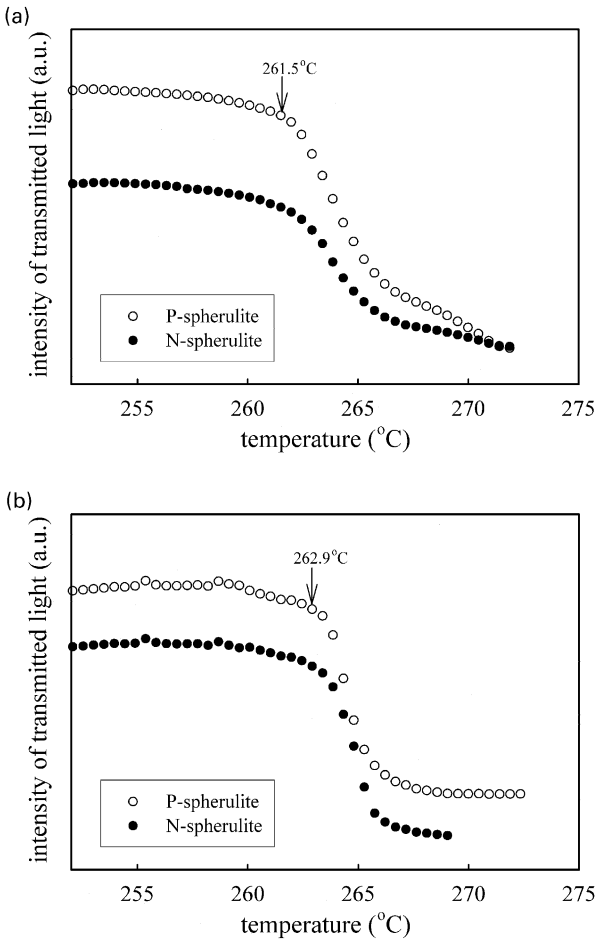

Fig. 5. Variation of the transmitted light intensity of P-spherulites and N-spherulites during heating of (a) neat sPS and (b) sPS/aPS = 50/50 blends melt-crystallized at T_c = 252 °C. (cross-polars, heating rate = 10 °C/min).

measured intensity is found for both P- and N-spherulites. The disappearance of the intensity upturn is evident for 50/50 blends, implying the absence of the reorganization and/or recrystallization behavior during heating. When crystallized at T_c = 252 °C, only an evident intensity drop is detected for both neat sPS and 50/50 blends during heating scans, as shown in Fig. 5. From the results shown in Figs. 4 and 5, it is of interest to note that the intensity profiles during melting of P- and N-spherulites are the same, regardless of the crystallization temperature and the addition of aPS.

To determine melting temperature more precisely from POM results, the derivative of the measured intensity (I) with respect to temperature was calculated and plotted as a function of temperature. Fig. 6 gives the calculated results for neat sPS crystallized at T_c = 241 and 252 °C, respectively. Also given in Fig. 6 is the baseline obtained from the straight lines of low- and high-temperature extremes where no variation of transmitted light intensity should take place. Thus, melting is in progress if the calculated $-\mathrm{d}I/\mathrm{d}T$ curve is above the baseline. On the other hand, an increase of crystallinity is evident when the $-\mathrm{d}I/\mathrm{d}T$ curve is below the baseline. For sPS samples crystallized at 241 °C, reorganization (or recrystallization) is clearly defined starting from 260 to 264 °C where the calculated $-\mathrm{d}I/\mathrm{d}T$ values are lower than the baseline. This is similar with DSC results (Fig. 19, Ref. [15]) where a small exotherm is detected on heating sPS samples previously crystallized at T_c = 240 °C. It is evident that both P- and N-spherulites show exactly the same melting curves, implying that the same lamellar thickness (or perfection) is developed within P- and N-spherulites. The peak location of the melting curves is taken as the melting temperature, T_m. For neat sPS as shown in Fig. 6, two T_ms are found (258.1 and 269.4 °C) for samples crystallized at T_c = 241 °C, whereas only one apparent T_m is detected at 263.9 °C, accompanying with a less obvious T_m at 270.5 °C when crystallized at T_c = 252 °C. For sPS/aPS = 50/50 blends, Fig. 7 shows a comparison of melting curves obtained from POM as well as DSC at the same heating rate. Identical double-melting peaks located at 258.3 and 268.9 °C are observed for both P- and N-spherulites which are in good agreement with DSC results based on the

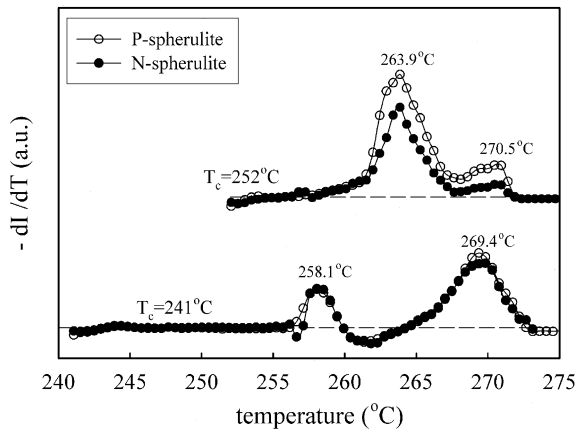

Fig. 6. Determination of melting temperatures of P- and N-spherulites of neat sPS melt-crystallized at T_c = 241 and 252 °C (the broken lines denote the baseline).

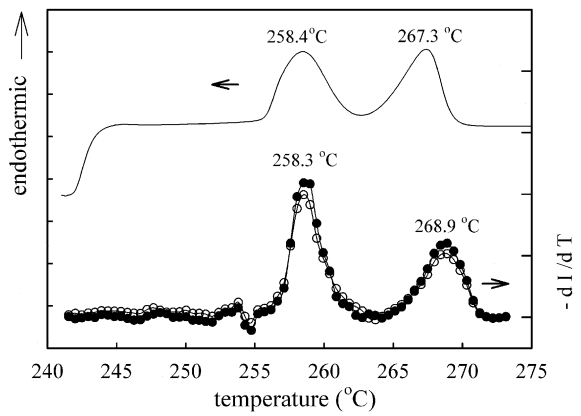

Fig. 7. A comparison of the melting behavior of sPS/aPS = 50/50 blend obtained from DSC and POM. The upper curve is DSC heating trace of the blend and the data points are obtained from POM for P-spherulites (open circles) and N-spherulites (filled circles). Prior to the heating trace at a rate of 10 °C/min, samples are melt-crystallized at T_c = 241 °C for 7 min.

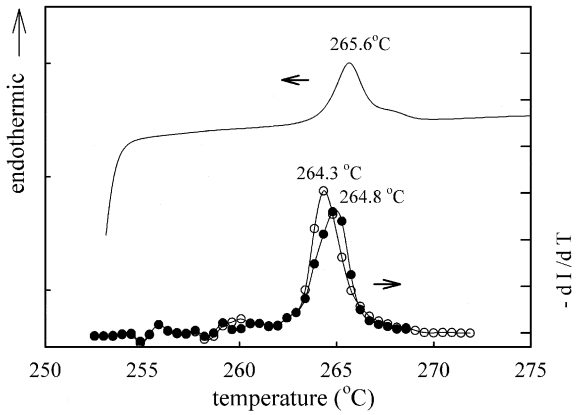

Fig. 8. A comparison of the melting behavior of sPS/aPS = 50/50 blend obtained from DSC and POM. The upper curve is DSC heating trace of the blend and the data points are obtained from POM for P-spherulites (open circles) and N-spherulites (filled circles). Prior to the heating trace at a rate of 10 °C/min, samples are melt-crystallized at T_c = 252 °C for 7 min.

enthalpies required for the crystal melting. For samples crystallized at T_c = 252 °C, an evident melting peak is observed from DSC and POM results, as shown in Fig. 8. Owing to different sample sizes and thermal environments used for DSC and POM experiments, respectively, slightly different values of T_m may be obtained. The small variation of T_m determined for P- and N-spherulites is attributed to the temperature resolution of measurement. Nevertheless, it is worthy to note that consistent melting curves can be deduced on a basis of light intensity measurements by POM, when compared with results by calorimetric techniques. To further improve results obtained from POM, however, the reduction of time intervals required to complete a recorded image is necessary, giving a finer temperature resolution and more precise determination of T_m. Present POM observations lead us to conclude that both P- and N-spherulites demonstrate the same melting behavior although the crystal growth rates are quite different from each other.

3.2. Lamellar morphology within spherulites

When semicrystalline polymers are crystallized from the melt, it has been established that spherulitic structures consisting of regular pack of lamellae are developed. According to Norton and Keller [25], two different categories of spherulites are normally observed, i.e. central multidirectional growth (category I) and sheaf-like unidirectional growth (category II). In category I, the central lamellar nuclei initiate the crystal growth in multiple directions to occupy the available space through branching and splaying, giving the dominant lamellae and leading to a gradual growth of spherical entities. Some subsidiary lamellae are developed later between the dominant lamellae, especially in the peripheral region of spherulites. In category II, on the other hand, a single lamellar crystal initiates the crystal growth in the lateral direction first, followed by the deposition of second lamellar nucleus over its fold surfaces. Thus, in addition to the growth in the lateral dimension (unidirectional) which is normally observed, the thickness increment in the fold direction is also evident due to the gradual depositions of new lamellar nuclei, leading to a sheaf-like structure (lamellar stack or bundle). Through branching and fanning in the intermediate stages of sheaves, a final spherical shape is developed, leaving a 'two eyes' feature within the spherulites.

When a non-crystallizing aPS diluent is added into sPS, segregation of aPS species into elongated domains upon sPS crystallization is evidently observed due to crystallization-induced phase separation, leading to a more open structure of the spherulites for detailed morphological observations (Fig. 9). Fig. 9 shows the internal microstructure of sPS/aPS = 50/50 spherulites probed by TEM. It is interesting to note that both category I and II as classified by Norton and Keller [25] are evidently observed in Fig. 9(a) and (b). In Fig. 9(a), spherulites in category I is verified where radiating sPS lamellar stacks grow in multiple directions and are branched consecutively, leaving the uncrystallizable aPS chains to form phase-separated domains. The non-spherical shape of segregated aPS domains verifies the occurrence of crystallization-induced phase separation. The second kind of spherulites (category II) is given in Fig. 9(b) where the 'two eyes' character due to the unidirectional growth of the

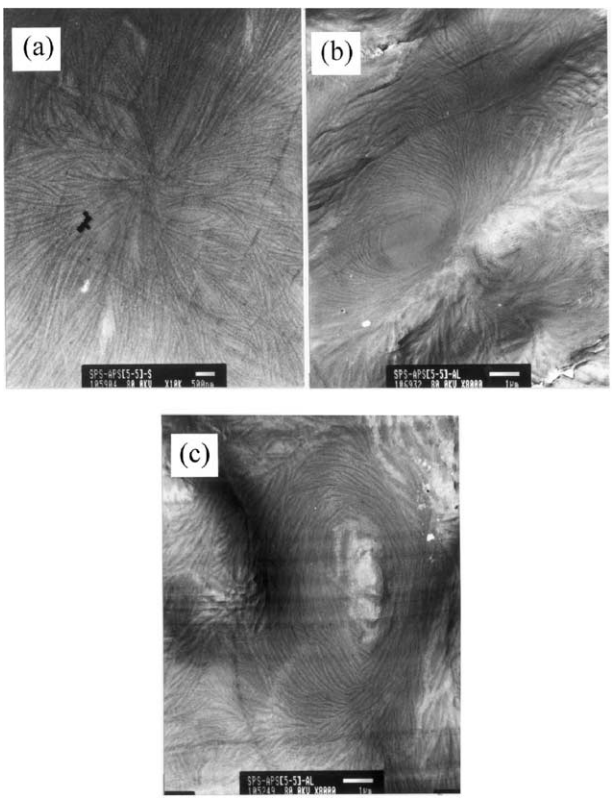

Fig. 9. Typical spherulitic morphology observed by TEM for sPS/aPS = 50/50 blends, (a) category I spherulite, (b) category II spherulite with 'two eyes' feature, and (c) new type of spherulite with 'one eye' feature.

initial lamellar stacks is clearly observed. In addition to the sPS spherulites of category I and II, spherulites of third kind are presented in Fig. 9(c) where many lamellar stacks are arranged more or less tangentially around a specific lamellar stack. Although the central portion is similar with the 'eye' character that category II spherulites possess, only 'one eye', however, is detected for this unique spherulite. Moreover, discontinuous and relatively short lamellar stacks are observed around the central 'eye' which is distinguished from the category II spherulites where continuous and long lamellar stacks are revealed, resulting from branching and fanning process during growth. For the unique spherulite shown in Fig. 9(c), it seems that many lamellar stacks simultaneously initiate individually and grow around a specific lamellar stack which will form the 'eye' feature later. After the impingement of neighboring lamellar stacks, a relatively compact and spherulite-like structure is developed, leaving that the probable mechanism for spherulitic growth is due to the gradual deposition of new lamellar nuclei over the outer pre-existing lamellae first, followed by the growth in the lamella' lateral direction.

SEM images of sPS/aPS = 50/50 blends are shown in Fig. 10 where the aPS component has been washed away with amyl acetate, leaving the voids of aPS segregated domains for easier observation of lamellar morphology within individual spherulites. Fig. 10(a) and (b) evidently shows the presence of spherulites in category I and II, respectively, which well resemble the corresponding TEM images in Fig. 9(a) and (b). Also noted in Fig. 9(b) is the occurrence of under-developed sheaf-like feature at the upper right-hand corner. This sheaf-like feature tends to grow more preferentially in the lateral direction of initial lamellar nuclei, resulting in an ellipsoidal entity and formation of axilites detected clearly under POM observation. When axilites are observed, the growth rate of long major axis indeed is relatively faster than that of the short minor axis. As discussed previously, these axilites are dominantly observed under POM at high T_c. In Fig. 10(c), a 'rose-like' spherulite is observed in the middle of the image within which the sPS lamellar stacks are arranged tangentially around a center hole filled possibly with aPS components prior to amyl acetate etching. Also noted in Fig. 10(c) is the simultaneous presence of spherulites classified into categories I and II at its right-hand side and upper left-hand corner, respectively. The morphological evidences of Figs. 9(c) and 10(c) strongly suggest the presence of third kind spherulites in addition to category I and II spherulites when sPS is crystallized.

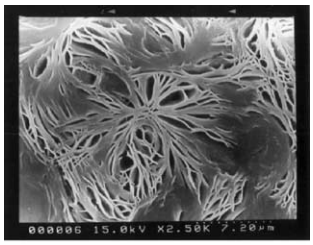

(a)

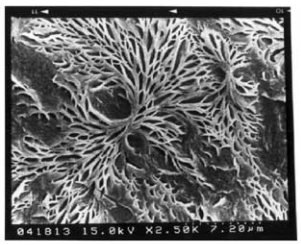

(b)

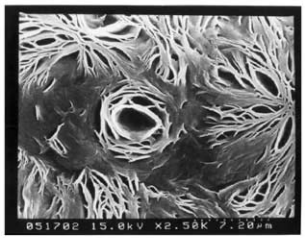

(c)

Fig. 10. Typical spherulitic morphology observed by SEM for sPS/aPS = 50/50 blends, (a) category I spherulite, (b) category II spherulite with 'two eyes' feature, and (c) new type of spherulite with 'one eye' feature.

3.3. Origin of negative spherulites

During isothermal crystallization at various temperatures, T_c, transition from P-spherulites to N-spherulites has been well known for nylon 6,6 and polypropylene (PP). For nylon 6,6, there is a T_c boundary below which P-spherulites are developed, whereas above which N-spherulites are observed during crystallization. This transition temperature where P-spherulites disappear and transform to the N-spherulites has been determined to be ca. 251 °C. On the basis of micro-beam X-ray studies, Keller [18] showed that the *c*-axis of nylon 6,6 crystals in P- and N-spherulites is tangential. The origin to lead the difference in the birefringence of spherulites is attributed to the orientation of the hydrogen-bonded (010) planes. The hydrogen-bonded plane is perpendicular to the spherulitic radius in N-spherulites and parallel in the P-spherulites. For PP, on the other hand, the origin of birefringent difference in spherulites is attributed to the presence of cross-hatching arrangement for parent (radiating) lamellae and daughter (branching) lamellae [19,26]. At low T_c, presence of predominant daughter lamellae is observed, leading to the P-spherulites. The level of lamellar cross-hatching is significantly reduced at high T_c, giving the appearance of N-spherulites only. Thus, the P- and N-spherulites are distinguished from each other by the degree of cross-hatching [19,26].

The situation encountered for sPS here is quite different from that for nylon 6,6 and PP. Firstly, simultaneous occurrence of P- and N-spherulites is observed in the wide

T_c range (as shown in Fig. 2) and there is no transformation from one type of spherulite to another during heating traces under POM observations. Secondly, there is no hydrogen-bond interaction between sPS molecular chains within the crystals to give strong polarizabilities perpendicular to the chains. Thirdly, no cross-hatched lamellar texture similar with what has been detected in PP spherulites is seen in the interior of sPS spherulites from our extensive TEM observations.

Generally speaking, the birefringent character of spherulites is mainly dependent on the orientation of lamellae which constitute the spherulites. Crystals of sPS orthorhombic system are uniaxial in refractive index ellipsoid; i.e. $n_a \sim n_b$ are the ordinary indices and n_c is the extraordinary index where n_a, n_b and n_c are the refractive indices in the *a*-, *b*-, and *c*-axis, respectively. The intrinsic birefringence for sPS crystals is given by: $n_c - (n_a + n_b)/2$. Although the refractive indices in the three axis direction have not been reported yet in the literature, the intrinsic birefringence of sPS crystals can be estimated as follows. It has been pointed out that the intrinsic birefringence of the crystal will be lower than that of amorphous phase due to the internal field effects of the ordered lattice arrangement of neighboring crystallizing chains [27,28]. The intrinsic birefringence of aPS has been widely reported previously. Due to the presence of polarizable phenyl substituent, the refractive index in aPS backbone chain direction is smaller than that perpendicular to the chain axis, leading to a negative intrinsic birefringence. sPS has the same repeating units as aPS except for the difference in the tacticity. Thus, the intrinsic birefringence of sPS in amorphous state should be similar with aPS. Indeed, a value of -0.11 was obtained for the intrinsic birefringence of amorphous sPS from the dynamic birefringence measurements [29], which is rather close to the reported value for aPS, -0.16 [30]. From above arguments, a negative intrinsic birefringence for sPS crystals is expected, leading to $n_c < n_a$ or n_b.

Since the diameters of spherulites are rather smaller, 30 μm at most for P-spherulites and 15 μm for N-spherulites as shown in Fig. 3, it is not an easy task to probe the orientation of crystals inside the spherulites using the micro-beam X-ray diffraction techniques. However, electron microscopy can provide sufficient resolution of the lamellar arrangement within the spherulites to verify previous arguments regarding the origin of the different spherulite types. The sPS backbone chains are along the *c*-axis direction in the orthorhombic crystals. When lamellae grow radially to form spherulites (Figs. 9(a) and (b)) which are predominantly observed, the individual sPS chains (crystal *c*-axis) are folded back and forth tangentially within spherulites, resulting in the development of P-spherulites. Thus, the growth of P-spherulites follows the conventional theory of crystal growth mechanism, i.e. its growth rate is associated with the lateral growth rate of lamellar crystals. In other words, a two-dimensional nucleus first forms on the growing front of a lamella, followed by the spreading

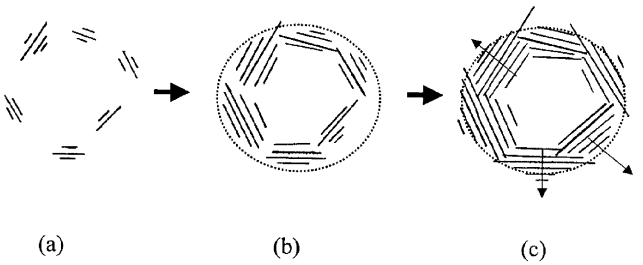

Fig. 11. Schematic representation of the formation process of a negative spherulite. (a) Several lamellar stacks are initiated and grow around a particular center. In this stage, not only the lateral growth of individual lamella is observed but also an increase of lamellar number in each stack is evident. (b) A spherical shape of lamellar-stack aggregates is apparently developed after impingement of neighboring lamellar stacks which leads to the first appearance of N-spherulite. (c) Measured growth rate of N-spherulite is mainly determined by the formation of lamellar nuclei parallel to the existing lamellae at the outer surface of the spherulite.

growth of crystals on the substrate. It has been recognized that crystal growth rate is dependent on the interplay of two factors, i.e. the surface (secondary) nucleation rate and the substrate completion rate at the growing front.

In contrast, N-spherulites should be composed of lamellae packed perpendicularly to the spherulitic radius, as shown in Fig. 9(c). It leads that the crystal *c*-axis lies more or less along the radius direction and a smaller n_r is expected, when compared to n_t. It is considered that the formation of N-spherulites is relevant to a particular arrangement of lamellar nuclei with respect to their neighboring ones at the very early stage of crystallization, as shown in Fig. 11(a). Not only will the lamellar stacks grow dominantly in the lateral dimensions but also more new lamellae are stacked gradually, forming more thick stack layers. Impingement of lamellar stacks takes place eventually, as shown in Fig. 11(b), leading to an apparently spherical feature composed of lamellar aggregates packed relatively tangentially. This gives the first appearance of discernible N-spherulites under POM observations. Since the lamellar arrangement within this N-spherulite is rather loose and irregular, a fainter and less birefringent character is observed when compared to the P-spherulite where a more compact lamellar texture is developed inside. Moreover, it takes certain induction time for a N-spherulite to form a relatively spherical entity, which accounts for its late appearance under POM, compared to P-spherulites. As shown in Fig. 11(c), due to the hindrance of neighboring stacks the lateral growth of lamellae is greatly limited. At this stage, growth of the N-spherulite will depend mainly on the nucleation rate of new lamellar (three-dimensional) nuclei parallel to the already-existing lamellae at the growing spherical surface of the spherulite. The three-dimensional lamellar nuclei could be developed by the loose loop (or cilia) of polymer chains which is still remained within melt although the rest of chain segments have already been crystallized into the neighboring lamella. Apparently, secondary nucleation which is prevailing for P-spherulites

(and P-axilites) indeed presents a smaller free energy barrier to produce stable nuclei than primary nucleation due to a less surface free energy required for nucleation. It leads to the present observations that the measured growth rate of P-spherulites is larger than that of N-spherulites at a given T_c, as shown in Fig. 1.

4. Conclusions

When melt-crystallized, sPS and its blends with aPS can develop into three different morphologies at the micrometer scale, i.e. P-axilites, P-spherulites and N-spherulites at a given crystallization temperature. The crystal lattice of crystallized samples was characterized to be orthorhombic β' modification using WAXD. The linear growth rates, measured by a POM, of P-axilites and P-spherulites are the same and are about two times larger than that of the faint N-spherulites. By measuring the variation of the transmitted light intensity under cross-polars during heating in a hot stage, melting behavior of individual P- and N-spherulites was traced, respectively. Results show that both P- and N-spherulites show exactly the same melting behavior; double-melting peaks at low crystallization temperatures, whereas single-melting peak at high crystallization temperatures which resembles the DSC heating traces. TEM was also used to probe the morphology at the nanometer scale to reveal the internal microstructure of the spherulites. Results show that radial orientation of the lamellar stacks is observed in the P-spherulites, whereas relatively tangential arrangement of lamellar stacks is detected in the N-spherulites. Similar morphological evidence is provided from the exhaustive SEM images.

Acknowledgments

The financial support of National Science Council of Republic of China (NSC89-2216-E-006-050) is gratefully acknowledged.

References

[1] Guerra G, Vitagliano VM, Rosa CD, Petraccone V, Corradini P. Macromolecules 1990;23:1539.
[2] Hong SM, Choi SH, Lee CH, Hwang SS, Kim KU, Cho I. Polym J 2000;32:187.
[3] Cartier L, Okihara T, Lotz B. Macromolecules 1998;31:3303.
[4] Tosaka M, Hamada N, Tsuji M, Kohjiya S. Macromolecules 1997;30:6592.
[5] Wu HD, Wu ID, Chang FC. Macromolecules 2000;33:8915.
[6] Zimba CG, Rabolt JF, English AD. Macromolecules 1989;22:2867.
[7] Barnes JD, McKenna GB, Landers BG, Bubeck RA, Bank D. Polym Engng Sci 1997;37:1480.
[8] Chatani Y, Shimane Y, Ijitsu T, Yukinari T. Polymer 1993;34:1625.
[9] Rosa CD. Macromolecules 1996;29:8460.
[10] Ho RM, Lin CP, Hseih PY, Chung TM, Tsai HY. Macromolecules 2001;34:6727.
[11] Cimmino S, Pace ED, Martuscelli E, Silvestre C. Polymer 1991;32:1080.
[12] Woo EM, Wu FS. J Polym Sci, Polym Phys Ed 1998;36:2725.
[13] Cimmino S, Pace ED, Martuscelli E, Silvestre C. Polym Commun 1991;32:251.
[14] Cimmino S, Pace ED, Martuscelli E, Silvestre C. Polymer 1993;34:2799.
[15] Wang C, Hsu YC, Lo CF. Polymer 2001;42:8447.
[16] López LC, Cieslinski RC, Putzig CL, Wesson RD. Polymer 1995;36:2331.
[17] Kit KM, Schultz JM. J Polym Sci, Polym Phys Ed 1998;36:873.
[18] Keller A. J Polym Sci 1955;17:351.
[19] Awaya H. Polymer 1988;29:591.
[20] Woo EM, Wu FS. Macromol Chem Phys 1998;199:2041.
[21] Wunderlich B, Macromolecular physics, vol. 1. New York: Academic Press; 1973.
[22] Magill JH. J Polym Sci 1966;4:243.
[23] Ding Z, Spruiell JE. J Polym Sci, Polym Phys Ed 1996;34:2783.
[24] Pratt CF, Hobbs SY. Polymer 1976;17:12.
[25] Norton DR, Keller A. Polymer 1985;26:704.
[26] Padden Jr. FJ, Keith HD. J Appl Phys 1966;37:4013.
[27] Dumbleton JH. J Polym Sci 1968;6:795.
[28] Stein RS. J Polym Sci 1969;7:1021.
[29] Inoue T, Ryu DS, Osaki K, Takebe T. J Polym Sci, Polym Phys Ed 1999;37:399.
[30] Stein RS. J Appl Phys 1961;32:1280.